

Bioethanol lignin-rich residue from olive stones for electrospun nanostructures development and castor oil structuring

José F. Rubio-Valle, José E. Martín-Alfonso, María E. Eugenio, David Ibarra, José M. Oliva, Paloma Manzanares, C. Valencia



PII: S0141-8130(23)04941-3

DOI: <https://doi.org/10.1016/j.ijbiomac.2023.128042>

Reference: BIOMAC 128042

To appear in: *International Journal of Biological Macromolecules*

Received date: 19 July 2023

Revised date: 14 October 2023

Accepted date: 9 November 2023

Please cite this article as: J.F. Rubio-Valle, J.E. Martín-Alfonso, M.E. Eugenio, et al., Bioethanol lignin-rich residue from olive stones for electrospun nanostructures development and castor oil structuring, *International Journal of Biological Macromolecules* (2023), <https://doi.org/10.1016/j.ijbiomac.2023.128042>

This is a PDF file of an article that has undergone enhancements after acceptance, such as the addition of a cover page and metadata, and formatting for readability, but it is not yet the definitive version of record. This version will undergo additional copyediting, typesetting and review before it is published in its final form, but we are providing this version to give early visibility of the article. Please note that, during the production process, errors may be discovered which could affect the content, and all legal disclaimers that apply to the journal pertain.

# **Bioethanol lignin-rich residue from olive stones for electrospun nanostructures development and castor oil structuring**

José F. Rubio-Valle<sup>a</sup>, José E. Martín-Alfonso<sup>a</sup>, María E. Eugenio<sup>b</sup>, David Ibarra<sup>b</sup>, José M. Olivac,  
Paloma Manzanares<sup>c</sup>, C. Valencia<sup>a\*</sup>

<sup>a</sup>Pro<sup>2</sup>TecS – Chemical Product and Process Technology Research Center. Department of Chemical Engineering and Materials Science. Universidad de Huelva. ETSI. Campus de “El Carmen”, Huelva 21071, Spain

<sup>b</sup>Instituto de Ciencias Forestales (ICIFOR-INIA, CSIC), Ctra de la Coruña Km 7.5, Madrid 28040, Spain

<sup>c</sup>Biofuels Unit, Renewable Energies Division, CIEMAT. Avda. Complutense 40, Madrid 28040, Spain

\* Author to whom correspondence should be addressed:

Prof. C. Valencia, Pro<sup>2</sup>TecS – Chemical Product and Process Technology Research Center. Dept. Chemical Engineering and Materials Science. ETSI. Campus de “El Carmen”, Universidad de Huelva. Huelva 21071, Spain

Phone: +34959218201, e-mail: barragan@uhu.es

38 **Abstract**

39 This work describes the chemical and structural characterization of a lignin-rich residue from  
40 the bioethanol production of olive stones and its use for nanostructures development by  
41 electrospinning and castor oil structuring. The olive stones were treated by sequential  
42 acid/steam explosion pretreatment, further pre-saccharification using a hydrolytic enzyme, and  
43 simultaneous saccharification and fermentation (PSSF). The chemical composition of olive  
44 stone lignin-rich residue (OSL) was evaluated by standard analytical methods, showing a high  
45 lignin content (81.3 %). Moreover, the structural properties were determined by Fourier  
46 transform infrared spectroscopy, nuclear magnetic resonance, and size exclusion  
47 chromatography. OSL showed a predominance of  $\beta$ - $\beta'$  resinol, followed by  $\beta$ -O-4' alkyl aryl  
48 ethers and  $\beta$ -5' phenylcoumaran substructures, high molecular weight, and low S/G ratio.  
49 Subsequently, electrospun nanostructures were obtained from solutions containing 20 wt.%  
50 OSL and cellulose triacetate with variable weight ratios in N, N-dimethylformamide/Acetone  
51 blends and characterized by scanning electron microscopy. Their morphologies were highly  
52 dependent on the rheological properties of polymeric solutions. Gel-like dispersions can be  
53 obtained by dispersing the electrospun OSL/CT bead nanofibers and uniform nanofiber mats in  
54 castor oil. The rheological properties were influenced by the membrane concentration and the  
55 OSL:CT weight ratio, as well as the morphology of the electrospun nanostructures.

56

57 **Keywords:** lignin, olive stones, cellulose triacetate, electrospinning, gel-like dispersion,  
58 rheology

59

60

61

62

## 63 1. Introduction

64 Lignocellulosic biomass (LB) can be transformed into fuels and value-added products  
65 in a biorefinery approach [1]. This new production model is a sustainable way to diminish our  
66 dependence on fossil fuels and mitigate global warming, based on the abundance, wide  
67 distribution, low cost, and non-competition with food of LB to be used as alternative feedstock  
68 [2]. Among the lignocellulosic sources that could be employed in a lignocellulosic biorefinery,  
69 olive stones (OS), a lignocellulosic by-product of the olive oil industry, can be contemplated as  
70 a suitable raw material. They are an abundant material in olive oil-producing countries such as  
71 Spain, where the production amounted to around 7.5 million tonnes in 2021 [3]. Taking into  
72 account that OS are around 10 % of the olive weight, the amount of these residues generated  
73 per year is approximately 750,000 tonnes. OS are removed from the olive fruit in the olive  
74 plant, the olive-oil pomace facility, or in both, depending on the local process operation. This  
75 residue has been usually used as fuel in small industries and domestic boilers in a changing  
76 situation that depends on the energy market conditions and the environmental regulations for  
77 its use as a solid fuel [4]. Thus, the valorization of OS in the context of lignocellulosic  
78 biorefineries would be of great interest to provide an alternative use for this by-product.

79 OS have been studied as promising raw material for the production of sugars to obtain  
80 advanced biofuels such as bioethanol and further value-added compounds such as xylitol and  
81 furfural [5]. The significance of the utilization of lignocellulosic residues to produce bioethanol  
82 is currently strengthened by the objectives of the updated Renewable Energy Directive of the  
83 European Commission [6]. Among the technologies developed so far to produce bioethanol  
84 from LB, the biochemical pathway represents the most favourable [7]. Briefly, this technology  
85 involves the release of the fermentable sugars contained in the biomass in the form of  
86 carbohydrates (cellulose and hemicellulose) after a pretreatment followed by an enzymatic  
87 hydrolysis step and a subsequent step of fermentation to ethanol [1]. Together with ethanol as

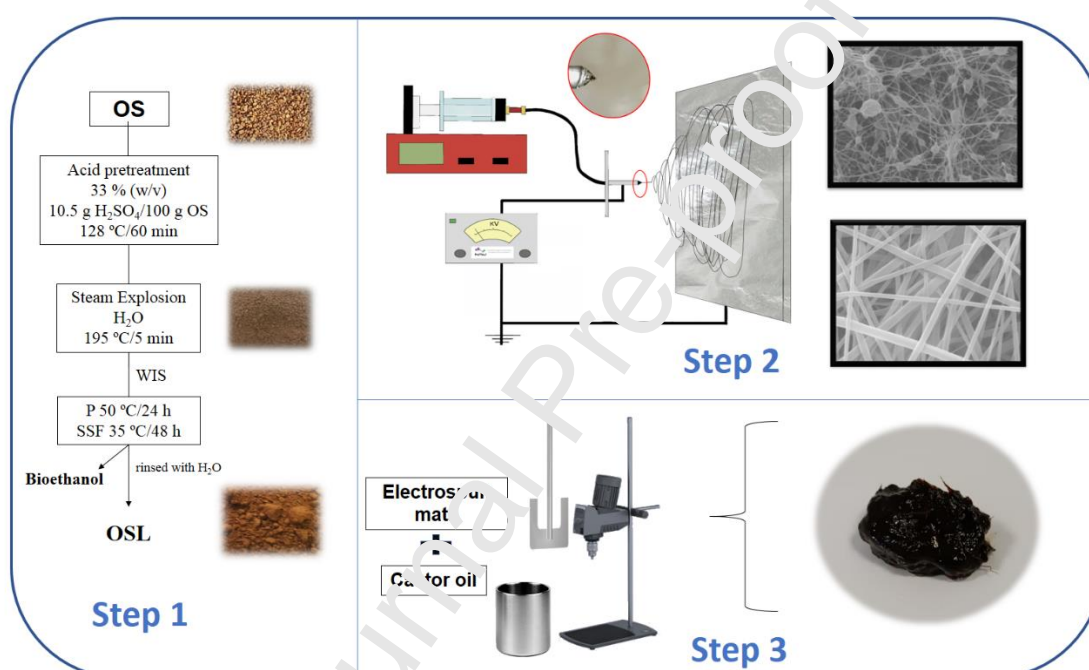
88 the main product, a lignin-rich residue is generated in this process, which in most cases is used  
89 as a solid fuel in the facility to produce heat and electricity for the process itself [8]. Lignin is  
90 a complex polymeric structure that results from the oxidative coupling of guaiacyl (G) (from  
91 coniferyl alcohol), p-hydroxyphenyl (H) (from p-coumaryl alcohol), and syringyl (S) (from  
92 sinapyl alcohol) phenylpropane units, producing carbon-carbon and aryl ether chemical bonds  
93 [9]. The high carbon content and aromatic structure of lignin, among others, make this  
94 lignocellulosic component an interesting raw material for high value-added chemicals and  
95 materials production [10], thereby increasing the competitiveness and sustainability of  
96 bioethanol production.

97         One possible way to revalorize these lignin-rich residues is to use them as a thickening  
98 or structuring agent of castor oil to produce gel-like dispersions. This is justified as a new way  
99 of revalorization and is in line with the new strategic routes that are based on the production of  
100 renewable biological resources and the conversion of these resources into high-value-added  
101 products [11,12]. In previous research, we have developed environmentally friendly gel-like  
102 dispersions in an attempt to imitate the frictional properties of conventional lubricating greases  
103 [13–15]. Then, growing environmental awareness has led to the substitution of petroleum-based  
104 components with renewable materials. For instance, the lubricant industry is not only  
105 substituting conventional mineral oils with vegetable oils or glycerol esters [16,17] but also  
106 chasing the development of lubricating greases obtained by using environmentally friendly oil  
107 structuring and thickening agents to replace metallic soaps, lithium soaps, mainly, with specific  
108 rheological properties. Therefore, new oil structuring agents based on renewable materials are  
109 needed to solve the existing technical and environmental requirements. Among the different  
110 biopolymers studied as oil thickening agents, lignin stands out as a promising alternative after  
111 chemical modifications such as functionalization with isocyanates [18,19], acetyl [15] or epoxy  
112 [20,21] groups promoting the formation of physical or chemical gels by generating covalent

113 bonds between the hydroxyl groups of lignin and the vegetable oil. However, although these  
114 final formulations may be inert and non-toxic, their processing involves the use of non-  
115 environmentally friendly chemicals and solvents. The main difficulty in this regard is to select  
116 and develop suitable processing and/or pretreatment protocols for the biopolymer that facilitate  
117 efficient interaction with the vegetable oil. A possible solution to overcome this difficulty is to  
118 obtain lignin-rich residues-based nanostructures. They present a high porosity and a high area-  
119 to-volume ratio that can lead to the development of a three-dimensional network with an  
120 outstanding ability to enhance the physical interactions of the thickening agent and the  
121 vegetable oil [22–24]. In this regard, electrospinning is one of the most important and widely  
122 used techniques for nanofabrication [25], due to the demand for materials with nanoscale  
123 dimensions. Thus, it becomes one of the most attractive processes thanks to the ability to  
124 transform a wide range of materials into nanostructures at a low cost and with relative  
125 simplicity. Several authors have studied the electrospinning process employing lignocellulosic  
126 materials [26,27]. It is worth mentioning the studies of Dallmeyer et al. [28,29], Borrego et al.  
127 [24,27] and García-Fuentevilla et al. [30,31], where a second polymer is used as a dopant  
128 because lignin alone does not create enough entanglements of the polymeric chains within the  
129 solution and, therefore cannot generate micro and/or nanometric fibers size. In this sense, the  
130 use of cellulose derivatives as a co-spinning polymer stands out due to they generate fibers with  
131 relative ease and with properties such as its biocompatibility and high crystallinity, in addition  
132 to come from a renewable resource [32–34].

133 This work investigates the valorization of a lignin-rich residue from bioethanol  
134 production of olive stones as a structuring agent of castor oil, through the development of  
135 nanostructures with cellulose triacetate in an electrospinning process (Figure 1). The chemical  
136 structure of this residue was determined by means of  $^1\text{H}$  and  $^{13}\text{C}$  nuclear magnetic resonance  
137 (NMR), two-dimensional NMR (2D NMR), Fourier-transform infrared (FTIR) spectroscopy

138 and size exclusion chromatography (SEC). In addition, the chemical composition was evaluated  
 139 by standardized analytical methods. On the other hand, the nanostructures obtained by the  
 140 electrospinning process of olive stone lignin-rich residue (OSL)/cellulose triacetate (CT)  
 141 solutions in a mixture of N,N Dimethylformamide (DMF) and acetone (Ac) were likewise  
 142 assessed by scanning electron microscopy (SEM). The rheological properties of the derived  
 143 gel-like dispersions were associated with the morphological features of the electrospun  
 144 nanostructures.



145 **Figure 1.** Schematic diagram of the valorization of bioethanol lignin-rich residue from olive  
 146 stones as a structuring agent for castor oil, by developing nanostructures with cellulose  
 147 triacetate in an electrospinning process.

149

## 150 2. Materials and Methods

### 151 2.1. Raw material and chemicals

152 Olive stones (OS), with a particle size ranging from 1-3 mm and moisture content of  
 153 8%, were supplied by a local company in Jaen (Spain). The material showed the following

154 chemical composition (dry weight basis): 20.9 % cellulose, 26.0 % hemicelluloses, 35.6 %  
155 lignin, 6.3 % extractives, 0.6 % ash, and 5.9 % acetyl groups [5].

156 Cellulose triacetate (CT) ( $M_n=100,000$  g/mol) was provided by Merck Sigma-Aldrich  
157 S.A. (Darmstadt, Germany) and used as a dopant in the polymeric solution to improve the  
158 electrospinning process. In addition, N, N-Dimethylformamide (DMF, purity 99.8 %) and  
159 acetone (Ac, purity 99.1 %), supplied by Merck Sigma Aldrich S.A. (Darmstadt, Germany)  
160 were used as solvents for the preparation of the solutions utilized in electrospinning.

161 Finally, all other chemicals were reagent-grade and purchased from Panreac (Spain) and  
162 Merck Sigma-Aldrich (Darmstadt, Germany). Castor oil from Guinama (Valencia, Spain) was  
163 used as an oil medium to prepare gel-like dispersions. The main physical properties and fatty  
164 acid composition of castor oil can be found elsewhere [35].

165

## 166 2.2. Production of lignin-rich residue

### 167 2.2.1. Pretreatment

168 OS were subjected to a two-step pretreatment according to Padilla-Rascón et al. [5].  
169 Firstly, an acid pretreatment was carried out at 128 °C with a solid/liquid ratio of 33 % (wt/v)  
170 and 10.5 g  $H_2SO_4/100$  g CS for 60 min in an autoclave. Secondly, a steam explosion  
171 pretreatment was performed at 195 °C for 5 min, using the solid fraction obtained in the acid  
172 pretreatment as feedstock. After that, the resulting two-step-pretreated material was filtered and  
173 the water-insoluble fraction (WIS) obtained was used as a substrate for bioethanol production  
174 in a Simultaneous Saccharification and Fermentation (SSF) process. The chemical composition  
175 of the WIS fraction was (dry weight basis): 35.4 % cellulose, 2.6 % hemicellulose, and 57.5 %  
176 lignin, determined according to the Laboratory Analytical Procedures for biomass analysis from  
177 the National Renewable Energies Laboratory [36], as described below in point 2.2.3.

178

### 179 2.2.2. Simultaneous Saccharification and Fermentation Process (SSF)

180 SSF was carried out in a two-step procedure. The first step consisted of a  
181 presaccharification of the WIS fraction at 20 % (wt/wt) concentration in sodium citrate buffer  
182 0.05 M at pH 4.8) in a Terrafors-IS bioreactor 15 L capacity (Infors HT, Switzerland) at 50 °C  
183 for 24 h (final amount of material introduced in the bioreactor was 1.5 Kg). An enzyme dose of  
184 30 FPU/g of a dry substrate of Cellic® CTec2 (Novozymes A/S, Bagsværd, Denmark) was  
185 used. After the presaccharification step, 0.5 Kg of the incubated materials was transferred to 1  
186 L Erlenmeyer flasks to undergo the fermentation stage in an orbital shaker at 150 rpm for 48 h.  
187 The temperature was set at 35 °C, and 1 g/L of *Saccharomyces cerevisiae* (“Ethanol Red”,  
188 Fermentis, France) of yeast was added with appropriate nutrients, which turned the process into  
189 SSF. Experiments were carried out in triplicate. After the fermentation time, the broth was  
190 filtered and the insoluble solids were rinsed with abundant water and used as lignin-rich residue  
191 (denoted hereinafter as olive stone lignin-rich residue (OSL)).

192

### 193 2.2.3. Chemical and structural characterization of lignin-rich residue

194 The chemical composition of OSL was analyzed according to the Laboratory Analytical  
195 Procedures for biomass analysis from the National Renewable Energies Laboratory [36].  
196 Following this methodology, after the acid hydrolysis of OSL, the acid-insoluble solid residue  
197 (Klason lignin) was recovered and weighted, whereas the liquid fraction that contains the  
198 monomeric sugars released from the remaining carbohydrates in OSL was analyzed by high-  
199 performance liquid chromatography (1260 HPLC, Agilent, Germany, equipped with a G1362A  
200 refractive index (RI) detector and an Agilent Hi-PlexPb column) [37]. Acid-soluble lignin  
201 content was also measured in the same liquid fraction by UV-Vis spectroscopy.

202 Fourier-transform infrared (FTIR) spectroscopy analysis was performed using a JASCO  
203 FT/IR-4200 (Jasco Inc., Japan) apparatus. OSL was dispersed in KBr to obtain disks that were

204 put in a sample holder. The spectra were collected in a wavenumber range of 400–4000  $\text{cm}^{-1}$ ,  
205 in the transmission mode, at 4  $\text{cm}^{-1}$  resolution [18].

206  $^{13}\text{C}$ – $^1\text{H}$  two-dimensional nuclear magnetic resonance (2D NMR) analysis of OSL  
207 (dissolved in 0.75 mL of deuterated dimethylsulfoxide, DMSO- $d_6$ ) was recorded at 25 °C in a  
208 Bruker Avance III 500 MHz NMR spectrometer (Billerica, MA, USA). HSQC (heteronuclear  
209 single quantum correlation) experiment was recorded according to previously reported  
210 operation conditions [18]. Residual DMSO (from DMSO- $d_6$ ) was used as an internal reference  
211 ( $\delta_{\text{C}}/\delta_{\text{H}}$  39.6/2.5 ppm). The abundance of  $\beta$ -O-4',  $\beta$ - $\beta'$  resinol,  $\beta$ -5' phenylcoumaran, and  
212 spirodienones substructures was estimated from  $\text{C}_\alpha$ - $\text{H}_\alpha$  correlations. Cinnamyl alcohol end-  
213 groups using  $\text{C}_\gamma$ - $\text{H}_\gamma$  correlations;  $\text{C}_{2,6}$ - $\text{H}_{2,6}$  correlations from S units; and  $\text{C}_2$ - $\text{H}_2$  correlations  
214 from G units were used to estimate the S/G lignin ratio.

215 The total phenols content of OS lignin-rich residue was measured using the Folin-  
216 Ciocalteu method modified according to Trujillo-López et al. [37].

217 Size exclusion chromatography (SEC) analysis of OSL was performed by HPLC (1260  
218 HPLC, Agilent, Germany); fitted with a G1315D diode array detector; and equipped with two  
219 columns (Phenomenex) coupled in series (GPC P4000 and P5000) and a safeguard column.  
220 The sample (dissolved to a final concentration of 0.5 g/L in NaOH (0.05 M)) was analyzed at  
221 254 nm using NaOH (0.05 M) as a mobile phase pumped at conditions reported by Borrero et  
222 al. [18]. Polystyrene sulfonated standards (peak average molecular weights of 4210, 9740,  
223 65,400, 470,000, PSS-Polymer Standards Service) were used for calibration purposes.

224

### 225 2.3. Electrospinning

226 The electrospun nanostructures were prepared based on previous studies [38]. OSL/CT  
227 solutions were manufactured in a DMF/Ac (1:2 v/v) mixture at a 20 wt.% total concentration  
228 with variable OSL:CT weight ratios (see Table 1), using a magnetic stirrer (650 rpm) at room

229 temperature (23 °C) for 24 h. Subsequently, the solutions were placed in centrifuge tubes and  
 230 centrifuged at 4500 rpm for 7 min to remove the residual impurities.

231 **Table 1.** Nomenclature for electrospun OSL/CT nanostructures with different weight ratios

Samples	OSL (%)	CT (%)
OSL100-CT0	100	0
OSL90-CT10	90	10
OSL80-CT20	80	20
OSL70-CT30	70	30
OSL60-CT40	60	40
OSL50-CT50	50	50

232 The nanofabrication with the OSL/CT solutions was performed in a DOXA  
 233 Microfluidics (Spain) electrospinning chamber. For this purpose, the syringe was attached to  
 234 the holder using a horizontal configuration and the high-voltage power supply provided a  
 235 potential difference of 17 kV. A 21G needle was used and 15 cm was established between the  
 236 collector plate and the tip of the needle. On the other hand, the OSL/CT solutions were pumped  
 237 at 0.6 mL/h. All experiments were performed at room temperature (~ 23 °C) and constant  
 238 relative humidity (45 ± 1 %).

239

#### 240 2.4. Characterization of the OSL/CT solutions

241 OSL/CT solutions were physicochemically characterized through surface tension,  
 242 electrical conductivity, and dynamic viscosity measurements. Surface tension measurements  
 243 were performed on a Sigma 703D tensiometer (Biolin Scientific, Sweden) using a Wilhelmy  
 244 platinum plate with a measuring range of 1-1000 mN/m. Electrical conductivity was measured  
 245 in a CE GLP31 conductivity meter (Crison, Spain) at 25°C, using a conductivity cell previously  
 246 calibrated with standards of known conductivity. Dynamic viscosity was performed at 25 °C,  
 247 with a RheoScope (Thermo Fisher Scientific, Waltham, USA) controlled-stress rheometer,

248 using plate and plate geometry (60 mm diameter, 1 mm gap) in a shear rate range of 1-300 s<sup>-1</sup>.

249 All measurements were made at least three times.

250

### 251 *2.5. Characterization of electrospun OSL/CT nanostructures*

252 The morphological properties of the electrospun nanostructures were determined by  
253 scanning electron microscopy (SEM) using a JXA-8200 SuperProbe microscope (JEOL,  
254 Japan), with a secondary electron detector at an accelerating voltage of 15 kV. Previously, a  
255 sputtering treatment with gold was carried out. An open-source program called DiameterJ was  
256 used to analyze the images of the nanostructures.

257

### 258 *2.6. Preparation and rheological characterization of the gel-like dispersions from electrospun*

#### 259 *OSL/CT nanostructures and castor oil*

260 The preparation of the gel-like dispersions from electrospun OSL/CT nanostructures  
261 were carried out based on previous studies [23]. The OSL/CT nanostructures obtained during  
262 the electrospinning process were carefully removed from the collecting plate with the help of  
263 tweezers and a spatula. The electrospun nanostructure (OSL90-CT10) was dispersed with  
264 concentrations of 5, 10 and 15 wt.% in castor oil at room temperature (~ 23 °C) for 24 h, using  
265 a controlled-rotational speed mixing device RW 20 from IKA (Staufen, Germany) equipped  
266 with an anchor-shaped impeller (75 rpm). In addition, several gel-like dispersions with variable  
267 OSL:CT weight ratios (90:10 to 50:50) were prepared at 5 wt.% in castor oil. The gel-like  
268 dispersions were stored at room temperature for further characterization.

269 Gel-like dispersions were rheologically characterized in a RheoScope (Thermo Fisher  
270 Scientific, Waltham, USA) controlled-stress rheometer, using a serrated plate and plate  
271 geometry (20 mm diameter, 1 mm gap). Small amplitude oscillatory shear (SAOS) tests were  
272 carried out, inside the linear viscoelastic region, in a frequency range of 0.03-100 rad/s at 25

273 °C. A stress sweep was previously performed to determine the linear viscoelastic regime.  
274 Viscous flow tests were conducted in a shear rate range of  $10^{-2}$ - $10^2$  s<sup>-1</sup> at 25 °C.

275

## 276 2.7. Statistical Analysis

277 An analysis of the variance (ANOVA) was performed using three replicates of each  
278 measurement independently. Furthermore, a comparison of means tests was performed to detect  
279 significant differences ( $p < 0.05$ ).

280

## 281 3. Results and discussion

### 282 3.1. Chemical and structural characterization of lignin-rich residue

#### 283 3.1.1. Chemical characterization

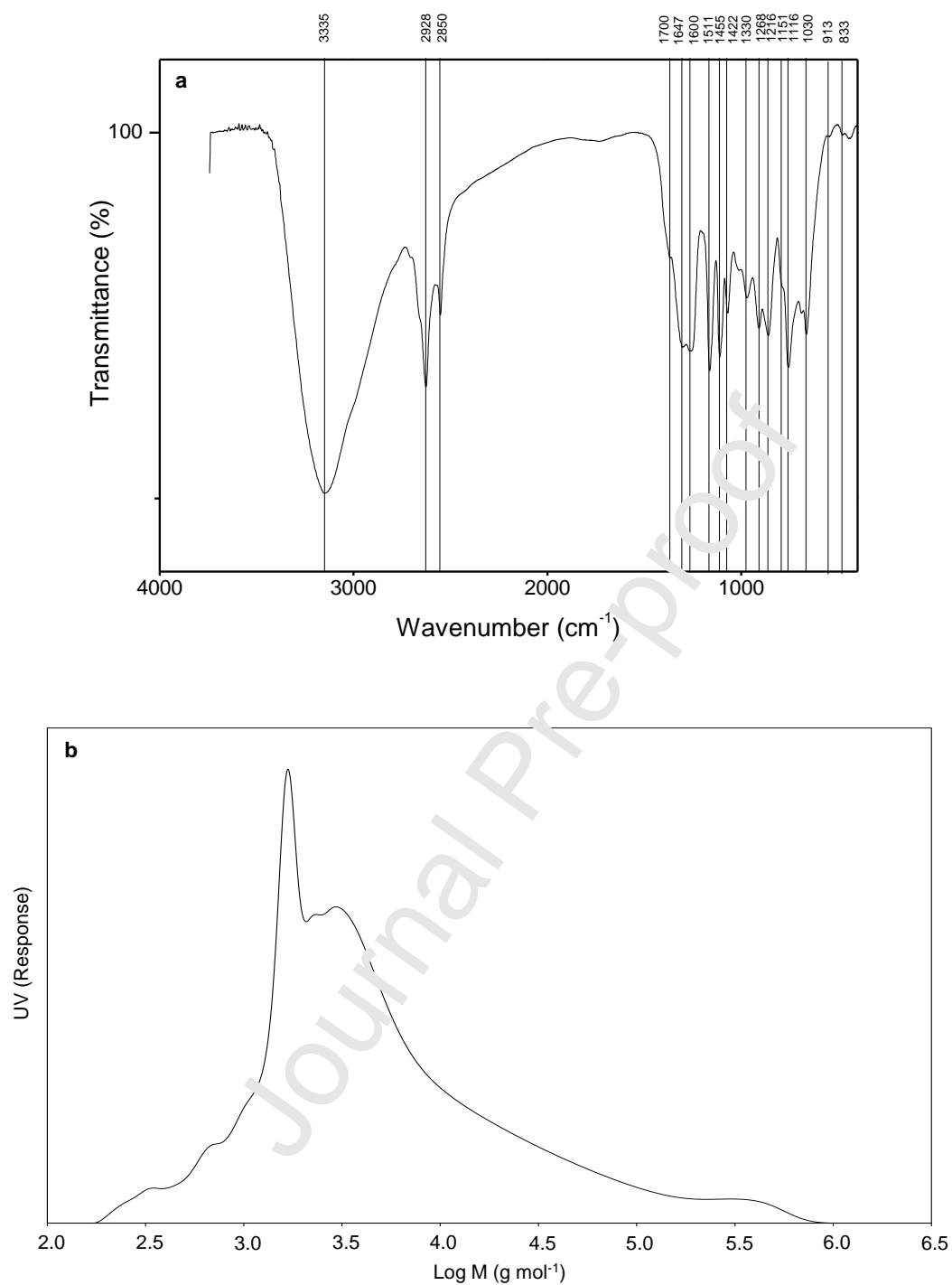
284 The chemical composition of OSL revealed a rather high lignin content (81.3 % total  
285 lignin; 80.6 % of acid-insoluble lignin and 0.7 % of acid-soluble lignin) compared to raw olive  
286 stones (35.6 % total lignin). This lignin concentration is due to the significant hydrolysis and  
287 solubilisation of hemicelluloses contained in olive stones material by acid pretreatment  
288 followed by steam explosion, as well as the glucose release in the subsequent enzymatic  
289 hydrolysis of the resulting pretreated material [39,40]. Despite the two-step pretreatment and  
290 the SSF, it was still possible to quantify certain carbohydrate content in the OSL, mainly glucan  
291 (12.2 %) and to a lesser extent xylan (1.1 %). It is well known that a part of the cellulose  
292 contained in LB is recalcitrant to the action of cellulolytic enzymes and that the carbohydrate  
293 content found in the residue depends largely on the severity of the pretreatment and the SSF  
294 conditions [41] Similar results have been reported in lignin-rich residues generated during  
295 bioethanol production from olive tree pruning, including steam explosion or acid catalysed  
296 steam explosion as pretreatments and subsequent saccharification and fermentation processes  
297 [42,43]. The presence of carbohydrate impurities detected in lignin may have a possible

298 influence on its valorization way, and based on the requirements of the target application some  
299 lignin purification may be necessary. Nonetheless, lignins with certain carbohydrate content  
300 have shown a positive effect on their subsequent valorization process as a thickening or  
301 structuring agent in vegetable oils by chemical functionalization [18,44].

302

### 303 *3.1.2. Structural characterization*

304 The characteristic functional groups of lignin-rich residue were evaluated by FTIR  
305 spectroscopy (Figure 2a). As with other lignin-rich residues generated during bioethanol  
306 production from olive-based materials, such as olive tree pruning [42,43], the OSL FTIR  
307 spectrum contains the typical lignin and carbohydrate bands. Regarding lignin, bands around  
308  $1330\text{ cm}^{-1}$ ,  $1268\text{ cm}^{-1}$  and  $833\text{ cm}^{-1}$ , associated with syringyl (S), guaiacyl (G) and *p*-  
309 hydroxyphenyl (H) units, respectively were observed, together with bands at  $1600\text{ cm}^{-1}$ ,  $1511$   
310  $\text{cm}^{-1}$ , and  $1422\text{ cm}^{-1}$  attributed to aromatic skeleton lignin vibrations. A wide O–H absorption  
311 peak at  $3335\text{ cm}^{-1}$  from lignin and carbohydrates was also clearly visible. Finally, two bands  
312 attributed to lignin oxidation could also be detected. On one side, a slight absorption at  $1700$   
313  $\text{cm}^{-1}$  was associated with unconjugated C=O groups. Nevertheless, carbonyl groups of  
314 hemicelluloses contained in OSL could also be contributing to this absorption [45]. On the other  
315 side, conjugated C=O groups at  $1647\text{ cm}^{-1}$  could be found, although this band could also be  
316 associated with amide bonds from hydrolytic enzymes used during saccharification [46].  
317 Concerning carbohydrates, cellulose and hemicellulose bands at  $1156\text{ cm}^{-1}$ ,  $1116\text{ cm}^{-1}$ , and  
318  $1030\text{ cm}^{-1}$  are visible, some of them overlapping lignin bands.



319

320 **Figure 2.** a) FTIR spectrum, 4000-750  $\text{cm}^{-1}$ , of olive stone lignin-rich residue and b) the  
321 molecular weight distribution of olive stone lignin-rich residue.

322 The main lignin and carbohydrate substructures were detected by 2D NMR analysis  
323 (HSQC spectra are displayed in Figure 3 and recognized substructures in Figure 4). OSL HSQC  
324 spectra show the typical lignin and carbohydrate signals (listed in Table 2), which were assigned

325 according to those described by different published studies on both native lignin and bioethanol  
 326 lignin-rich residues from olive tree pruning [42,43]. Despite the degradation of  $\beta$ -O-4' alkyl  
 327 aryl ethers (A),  $\beta$ - $\beta'$  resinol (B) and  $\beta$ -5' phenylcoumaran (C) native substructures reported by  
 328 several authors during acid and steam explosion pretreatments of aspen and poplar woody  
 329 materials as well as during enzymatic hydrolysis [47–49], the aliphatic-oxygenated region of  
 330 OSL HSQC spectrum still displayed correlation signals of them (Figure 3b). Moreover, possible  
 331 condensation reactions can also take place during these pretreatments [47,50]. Then, OSL  
 332 showed a predominance of  $\beta$ - $\beta'$  resinol substructures (42.1 % of the total inter-unit linkages),  
 333 followed by  $\beta$ -O-4' alkyl aryl ethers (31.4 %), and  $\beta$ -5' phenylcoumaran substructures (17.3  
 334 %). Other native lignin correlation signals were also visible, such as those corresponding to  
 335 spirodienones (E) and cinnamyl alcohol end-groups (I), with relative percentages of 9.1 % and  
 336 1.75 %, respectively.

337

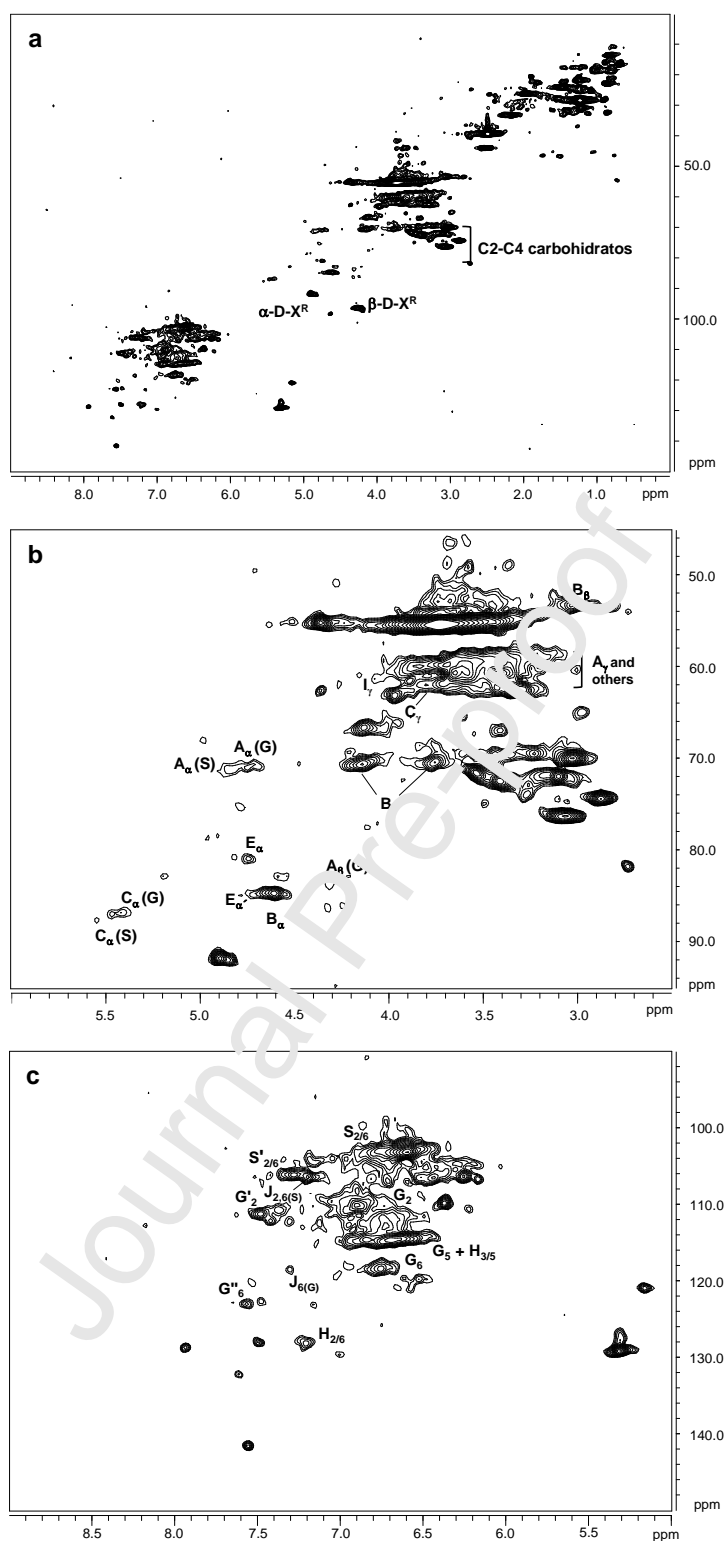
338 **Table 2** Assignment of main lignin and carbohydrates  $^{13}\text{C}$ - $^1\text{H}$  correlation peaks in the 2D  
 339 NMR HSQC spectra of olive stone lignin-rich residue

$\delta\text{C}/\delta\text{H}$ (ppm)	Assignment
54.0/3.04	$\text{C}_\beta\text{-H}_\beta$ , resinol substructures (B)
56.1/3.72	C-H, methoxyls (M-O)
60.6/3.38–3.64	$\text{C}_\gamma\text{-H}_\gamma$ , $\beta$ -O-4' substructures (A)
61.9/4.07	$\text{C}_\gamma\text{-H}_\gamma$ , cinnamyl alcohol end groups (I)
62.7/3.65	$\text{C}_\gamma\text{-H}_\gamma$ , phenylcoumaran substructures (C)
63.2/3.21–3.89	$\text{C}_5\text{-H}_5$ , xylan
71.3/3.76–4.18	$\text{C}_\gamma\text{-H}_\gamma$ , resinol substructures (B)
71.5/4.78	$\text{C}_\alpha\text{-H}_\alpha$ , $\beta$ -O-4' G unit (A)
72.1/4.87	$\text{C}_\alpha\text{-H}_\alpha$ , $\beta$ -O-4' S unit (A)
72.7/3.07	$\text{C}_2\text{-H}_2$ , xylan
74.0/3.26	$\text{C}_3\text{-H}_3$ , xylan
75.7/3.54	$\text{C}_4\text{-H}_4$ , xylan
81.6/4.72	$\text{C}_\alpha\text{-H}_\alpha$ , spirodienone substructures (E)
83.8/4.26	$\text{C}_\beta\text{-H}_\beta$ , $\beta$ -O-4' G unit (A)
85.3/4.74	$\text{C}_\alpha'\text{-H}_{\alpha'}$ , spirodienone substructures (E)
85.5/4.63	$\text{C}_\alpha\text{-H}_\alpha$ , resinol substructures (B)
87.5/5.42	$\text{C}_\alpha\text{-H}_\alpha$ , phenylcoumaran substructures G units (C)
88.5/5.59	$\text{C}_\alpha\text{-H}_\alpha$ , phenylcoumaran substructures S units (C)
92.3/4.89	reducing end (1–4) $\alpha$ -D-Xylp
97.3/4.27	reducing end (1–4) $\beta$ -D-Xylp
104.3/6.69	$\text{C}_{2,6}\text{-H}_{2,6}$ , S units (S)
106.2/7.12	$\text{C}_{2,6}\text{-H}_{2,6}$ , in cinamaldehyde end-groups S units (J)

106.7/7.32	C <sub>2,6</sub> -H <sub>2,6</sub> , oxidized (H-C <sub>α</sub> =O or H <sub>3</sub> C-C <sub>α</sub> =O) S units ( <b>S'</b> )
111.0/6.88	C <sub>2</sub> -H <sub>2</sub> , G units ( <b>G</b> )
111.0/7.38	C <sub>2</sub> -H <sub>2</sub> , oxidized (H-C <sub>α</sub> =O) G units ( <b>G'</b> )
115.0/6.74	C <sub>3,5</sub> -H <sub>3,5</sub> , <i>p</i> -hydroxyphenyl ( <b>H</b> )
115.2/6.42-6.81	C <sub>5</sub> -H <sub>5</sub> , G units ( <b>G</b> )
119.4/7.30	C <sub>6</sub> -H <sub>6</sub> , in cinamaldehyde end-groups <b>G</b> units ( <b>J</b> )
119.6/6.78	C <sub>6</sub> -H <sub>6</sub> , G units ( <b>G</b> )
123.6/7.51	C <sub>6</sub> -H <sub>6</sub> , oxidized (H <sub>3</sub> C-C <sub>α</sub> =O) G units ( <b>G''</b> )
128.3/7.19	C <sub>2,6</sub> -H <sub>2,6</sub> , <i>p</i> -hydroxyphenyl ( <b>H</b> )

---

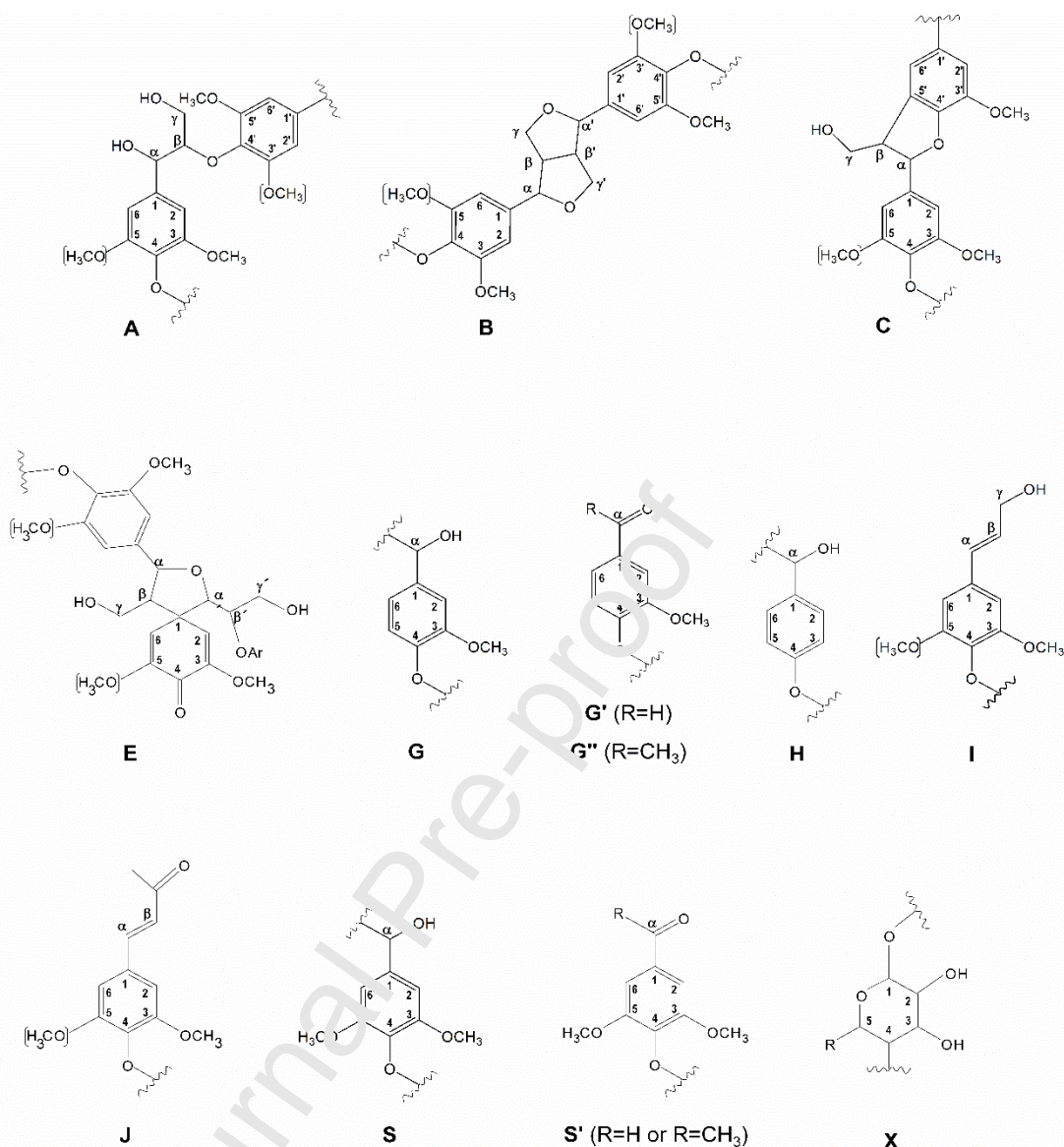
340 Finally, this aliphatic-oxygenated region of OSL also revealed carbohydrate signals  
341 (Figure 3b), either from hexose or pentose units, according to the chemical composition  
342 determined. These signals comprised mainly correlations of the xylan chain (X), together with  
343 the cross peaks for  $\alpha$ - and  $\beta$ -xylose reducing ends (Figure 3a).



344

345 **Figure 3.** 2D-NMR HSQC spectra of olive stone lignin-rich residue. a) whole spectrum,  $\delta_C/\delta_H$ 346 0.0–150.0/0.0–9.0 ppm; b) aliphatic oxygenated region,  $\delta_C/\delta_H$  45.0–95.0/2.5–6.0 ppm; and c)347 aromatic region,  $\delta_C/\delta_H$  90.0–150.0/5.0–9.0 ppm.

348           Regarding the aromatic region of the OSL HSQC spectrum (Figure 3c), the  
349 characteristic correlation signals of S, G, and H lignin units were seen, in the same way that  
350 FTIR analysis. From them, the S/G ratio calculated was 1.37, slightly higher than native lignin  
351 from olive tree pruning [51]. Moreover, several correlation signals corresponding to lignin  
352 oxidation could also be found, supporting the observations previously described by FTIR.  
353 These signals include those attributed to oxidized S units ( $S'_{2,6}$ ), such as syringaldehyde and  
354 acetosyringone, and those corresponding to oxidized G units endorsed to vanillin ( $G'_2$ ) and  
355 acetovanillone ( $G''_6$ ). On the other hand, signals found at  $\delta_C/\delta_H$  105.0/6.5, 112.8/6.7, and  
356 119.7/6.5 ppm were tentatively attributed to possible condensation reactions of lignin occurred  
357 during acid pretreatment or steam explosion [52]. Nevertheless, these correlation signals have  
358 also been associated with gallate and catechol-type structures [53] and most likely belong to  
359 condensed tannins consisting of gallo catechir units [54]. The presence of tannins has been  
360 recently reported in olive stones [55]. Finally, other native lignin units corresponding to  
361 cinnamaldehyde end-groups (J) in S units (sinapaldehyde end-groups) and in G units  
362 (coniferaldehyde end-groups), previously described in lignin from olive tree pruning [56,57],  
363 could also be identified in lignin from olive stone.



364

365 **Figure 4.** Main lignin and carbohydrate substructures identified in aliphatic oxygenated and  
 366 aromatic regions of olive stone lignin-rich residue: (A),  $\beta$ -O-4' alkyl-aryl ether; (B),  $\beta$ - $\beta'$   
 367 resinols; (C),  $\beta$ -5' phenylcoumarans; (E), spirodienones; (G), guaiacyl unit; (G'), vanillin; (G''),  
 368 acetovanillone; (H), p-hydroxyphenyl unit; (I), cinnamylalcohol end-groups; (J), cinnamyl  
 369 aldehyde end-groups; (S), syringyl unit; (S'), syringaldehyde or acetosyringone; (X),  
 370 xylopyranose (R, OH).

371

372 The molecular weight distribution of OSL is shown in Figure 2b. Several fractions are  
 373 displayed, including one with a broad peak of higher molecular weight and the other with a

374 narrow peak of lower molecular weight. Molecular weight and polydispersity values ( $M_w$ ,  
375 24965 Da;  $M_n$ , 2175 Da; PD, 11.4) could be calculated from this molecular weight distribution.  
376 These values are similar to those reported for lignins remaining in the insoluble residue from  
377 enzymatic hydrolysis of pretreated materials (from eucalypt, pine, and black locust woody  
378 materials) [18,58]. The remaining  $\beta$ -O-4' alkyl aryl ethers substructures after acid and steam  
379 explosion pretreatments can contribute to high molecular weight values, in spite of their  
380 degradation described during these processes [47], together with possible polymerization  
381 reactions, mainly via C–C bonds, which are also produced under these pretreatments [47]. In  
382 this sense, the high polydispersity value observed (11.4) could support that polymerization  
383 reactions have taken place during both acid and steam explosion pretreatments [59].

384

385 *3.2. Physicochemical properties of OSL/CT solutions and morphology of electrospun*  
386 *nanostructures.*

387 The skill to produce fibers during the electrospinning process lies in the  
388 physicochemical properties of the solutions and the fact that the polymer chains can achieve  
389 entanglements, as well as operating parameters (voltage, distance between the tip and collector,  
390 flow rate, humidity, and temperature). Some of these key intrinsic properties of the solution  
391 itself are dynamic viscosity, surface tension and electrical conductivity, which depend on the  
392 type of biopolymer, its concentration [22,27,30], and the solvent [60]. Table 3 displays the  
393 dynamic viscosity, surface tension and electrical conductivity values for the solutions prepared  
394 at different OSL:CT weight ratios. All the solutions present a Newtonian behavior in the range  
395 of the applied shear rate. As can be observed, the dynamic viscosity increases by increasing CT  
396 proportion, as previously studied with electrospun solutions of eucalyptus kraft lignin and  
397 cellulose acetate [38]. On the other hand, the incorporation of OSL and OSL/CT causes an  
398 increase in the surface tension of the DMF:Ac mixture (26.7 mN/m), which could be attributed

399 to an increase in the interaction between the solvent mixture and OSL. This is due to intra- and  
 400 intermolecular interactions between aromatic rings of lignin in DMF:Ac mixtures [61]. The  
 401 phenolic nature of OSL detected (the content of  $55 \pm 2.3$  mg GAE/g lignin-rich residue was  
 402 calculated by Folin-Ciocalteu method) leads to the enhancement of these interactions [62]. In  
 403 addition, the higher the amount of CT, the higher the surface tension values, because of the  
 404 hydrophobic character of CT. On the other hand, the electrical conductivity value of the solvent  
 405 blend was  $3.2 \mu\text{S}/\text{cm}$ , so the addition of OSL causes a similar effect to that presented in the  
 406 surface tension values, increasing the starting values of the solvent mixture, which could be  
 407 attributed to an increase in the number of ions due to the polarity presented by OSL [38].  
 408 However, when the OSL:CT weight ratio was decreased, it caused a decrease in the electrical  
 409 conductivity, given the lower molecular weight and more polar character of OSL as a  
 410 consequence of the chemical structure composed of phenolic and aliphatic hydroxyl and  
 411 carboxyl moieties, as shown above by FTIR and NMR.

412  
 413 **Table 3.** Dynamic viscosity, surface tension and electrical conductivity values for OSL/CT  
 414 solutions with different weight ratios

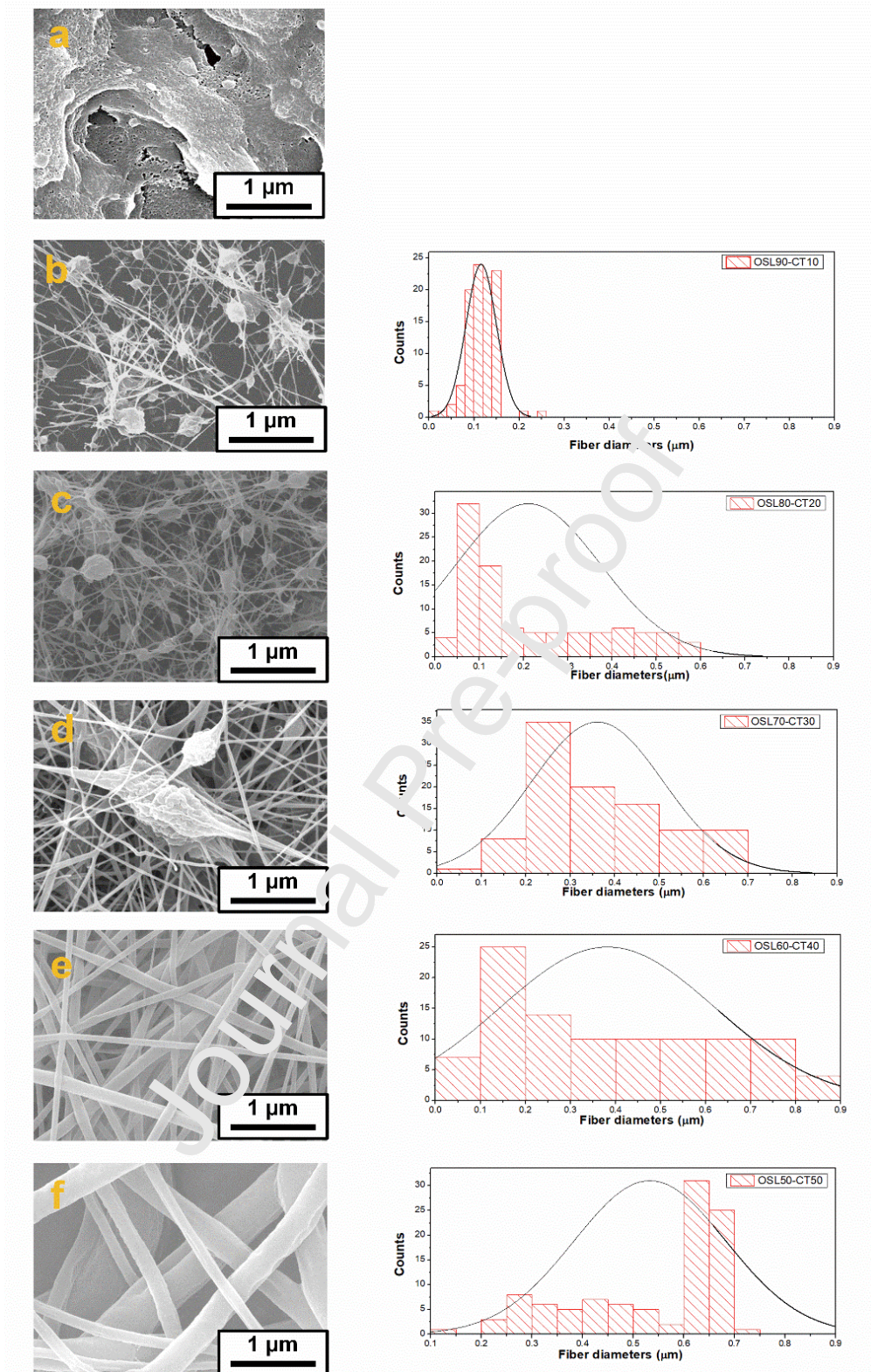
OSL:CT weight ratio	$\eta$ (mPa.s)	Surface tension (mN/m)	Electrical conductivity ( $\mu\text{S}/\text{cm}$ )
100:0	3.1 <sup>a</sup>	30.3 <sup>A</sup>	155.6 <sup>aA</sup>
90:10	21.4 <sup>b</sup>	32.1 <sup>B</sup>	135.2 <sup>bB</sup>
80:20	30.1 <sup>b</sup>	33.1 <sup>C</sup>	125.5 <sup>cC</sup>
70:30	55.3 <sup>c</sup>	34.3 <sup>C</sup>	117.8 <sup>cC</sup>
60:40	98.7 <sup>d</sup>	36.1 <sup>D</sup>	101.6 <sup>dD</sup>
50:50	209.7 <sup>e</sup>	37.9 <sup>E</sup>	92.1 <sup>eE</sup>

415 *Note: Values differing in the superscripts are significantly different ( $p < 0.05$ )*

416  
 417 Figure 5 shows the micrographs of the different electrospun nanostructures obtained by  
 418 SEM from the solutions prepared with variable weight ratios of OSL:CT. As can be observed,  
 419 the electrospinning of the solution without CT in the composition did not generate nanofibers,

420 but, on the contrary, the resulting nanostructures consisted of micrometer-sized particles, which  
421 are distributed forming agglomerates (Figure 5a). On the one hand, the microstructures of the  
422 solutions in which a lower amount of CT has been added (Figure 5b and 5c), presented  
423 nanometric fibers and particles, where fibers are intertwined with each other, and particles are  
424 interconnected. On the other hand, increasing the proportion of CT in the solution resulted in  
425 higher density and greater fiber abundance, as well as a slightly larger size of them (Figure 5d).  
426 Finally, in the micrographs of the systems in which 60:40 and 50:50 OSL:CT were used (Figure  
427 5e and 5f), it is observed that there are practically no OSL nanoparticles in the nanostructures,  
428 but they are integrated into the fibers themselves, forming a homogeneous structure. These  
429 results are because the increase of CT proportion in the solution causes an increase in the  
430 amount of entanglement of the polymer chains, due to the higher viscosity of the solution, as  
431 mentioned above. Moreover, these results agree with those obtained by other authors  
432 [27,28,38], showing the need for a second linear and high-molecular-weight polymer to act as  
433 a dopant given the inability of OSL to form entanglements between their polymer chains to  
434 generate fibers during the electrospinning process.

435



436

437 **Figure 5.** SEM images of electrospun nanostructures obtained from solutions with variable  
 438 OSL:CT weight ratios and fiber size distribution. a) OSL100-CT0, b) OSL90-CT10 c) OSL80-  
 439 CT20, d) OSL70-CT30 d) OSL60-CT40, f) OSL50-CT50.

440 The fiber size distribution and a Gaussian fit, which allows to obtain the average fiber  
441 size of the electrospun nanostructures generated during the electrospinning process, can also be  
442 observed in Figure 5. These distributions support the findings obtained from the micrographs,  
443 i.e., a significant increase in the average diameter of the fibers is obtained by increasing CT  
444 proportion. On the other hand, all the histograms of fiber diameter present a heterogeneous  
445 multidisperse distribution, except for the OSL90-CT10 system, which displays a homogeneous  
446 and monodisperse distribution as a consequence of the fact that the fibers intertwine the  
447 nanoparticles and these are not integrated into the fibers themselves, as occurs by increasing  
448 CT proportion.

449 Table 4 lists the average diameters of particles and fibers calculated from the size  
450 distributions of the electrospun nanostructures. As can be seen, there is a decrease in the mean  
451 particle size by increasing the CT proportion, because the particles are integrated into the fibers  
452 themselves. On the contrary, regarding the diameter of fibers, it is observed that the increase in  
453 the CT proportion leads to an increase in the average particle size. On the other hand, it is well  
454 known that an adequate electrospinnability of polymeric solutions can be accomplished with  
455 proper physicochemical properties (electrical conductivity, surface tension and dynamic  
456 viscosity) of the solution. Thus, by decreasing surface tension and increasing conductivity the  
457 jet formation and stretching of the nanofibers is facilitated, while high viscosity retards  
458 stretching, but prevents filament breakage then increasing fiber diameter [23,38]. Therefore,  
459 the lower the OSL:CT weight ratio, the higher the viscosity of the solution, favors an increase  
460 in fiber diameter. On the contrary, the higher the content of OSL, the higher the electrical  
461 conductivity and the lower the surface tension, which favors the thinning of the filaments and/or  
462 their rupture, essentially resulting in the formation of particles. These results are consistent with  
463 a previous work [38], where the electrospinning process of eucalyptus Kraft lignin and cellulose  
464 acetate solutions was studied.

465 **Table 4.** Average particle and fiber diameters of the OSL/CT electrospun nanostructures

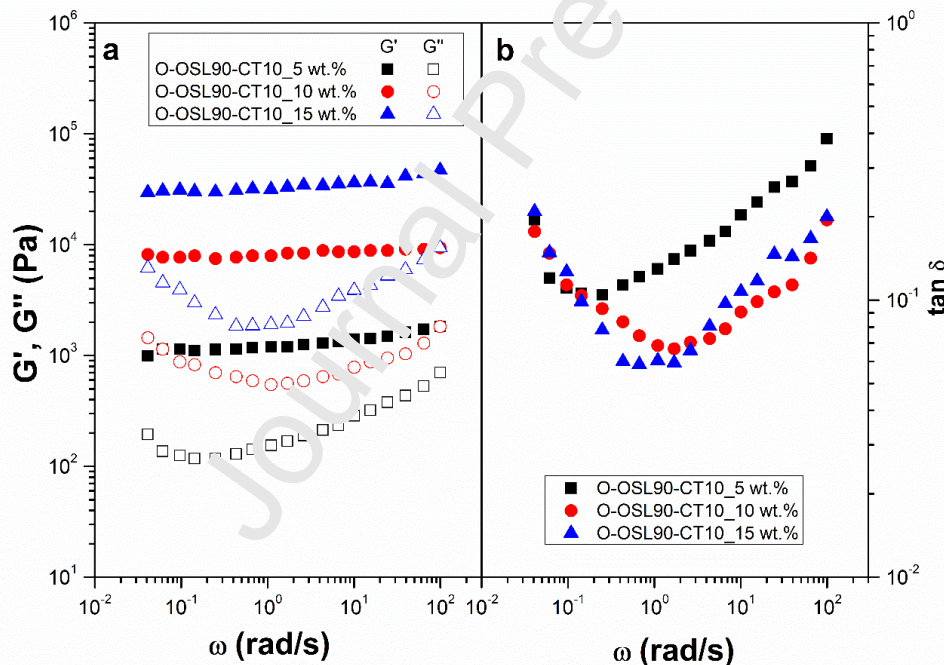
Sample Code	Average particle diameter ( $\mu\text{m}$ )	Average fiber diameter ( $\mu\text{m}$ )
OSL100-CT0	4.1	-
OSL90-CT10	1.7	0.12
OSL80-CT20	0.9	0.21
OSL70-CT30	0.6	0.34
OSL60-CT40	0.4	0.39
OSL50-CT50	-	0.52

466 *3.3. Castor oil structuring ability of electrospun OSL/CT nanostructures*

467 Several studies have already reported the production of gel-like dispersions employing  
 468 electrospun mats as a thickening agent in castor oil [22,60]. Borrego et al. [24] and Rubio-Valle  
 469 et al. [23,38] studied the ability to structure castor oil incorporating electrospun low-sulfonate  
 470 Kraft lignin/polyvinylpyrrolidone and eucalyptus Kraft lignin/cellulose acetate nanostructures,  
 471 respectively. The authors highlight that electrospun mats consisting only of micro or  
 472 nanometer-sized particles lead to the separation of the nanostructure from the castor oil over  
 473 time, because of weak interactions with the oil. On the other hand, electrospun mats formed by  
 474 micro or nanosized fibers result in stable gel-like dispersions due to physical interactions,  
 475 mainly intermolecular hydrophobic and Van der Waals forces, resulting from high surface  
 476 area/volume ratio of the nanofibers [38].

477 The electrospun nanostructure obtained from the OSL90-CT10 solution was dispersed  
 478 in castor oil with concentrations of 5, 10, and 15 wt.%, at room temperature, and the rheological  
 479 response was analysed. Figure 6a depicts the mechanical spectra of the resulting gel-like  
 480 dispersions, in the linear viscoelasticity range, as a function of the electrospun mats  
 481 concentration. The evolution of the storage,  $G'$ , and loss,  $G''$  moduli, with the frequency, is  
 482 characteristic of gel-like dispersions [63,64] and qualitatively similar to the three electrospun  
 483 mat concentrations, being  $G'$  always higher than  $G''$  in the whole frequency range studied. In  
 484 addition, a plateau region can be noticed at low and intermediate frequencies, while at high

485 frequencies a tendency to reach a crossing point between both moduli can be observed. Anyway,  
 486 the higher the electrospun mats concentration, the higher the viscoelastic functions, indicating  
 487 a stronger microstructural network. However, the relative elasticity was almost unaffected at  
 488 low frequencies, as can be seen in Figure 6b, where the plots of the loss tangent ( $\tan \delta = G''/G'$ )  
 489 versus frequency are shown. Only gel-like dispersions having low thickener concentration (5  
 490 wt.%) present higher values of the loss tangent at high frequency. As previously described [65],  
 491 the values of the SAOS functions depend basically on the content by weight of the thickening  
 492 agent, i.e. the content of the electrospun mats used in the gel-like dispersion. On the other hand,  
 493 to study the effect of the electrospun mats OSL:CT weight ratio on linear viscoelasticity and  
 494 viscous flow, a concentration of 5 wt.% was selected.

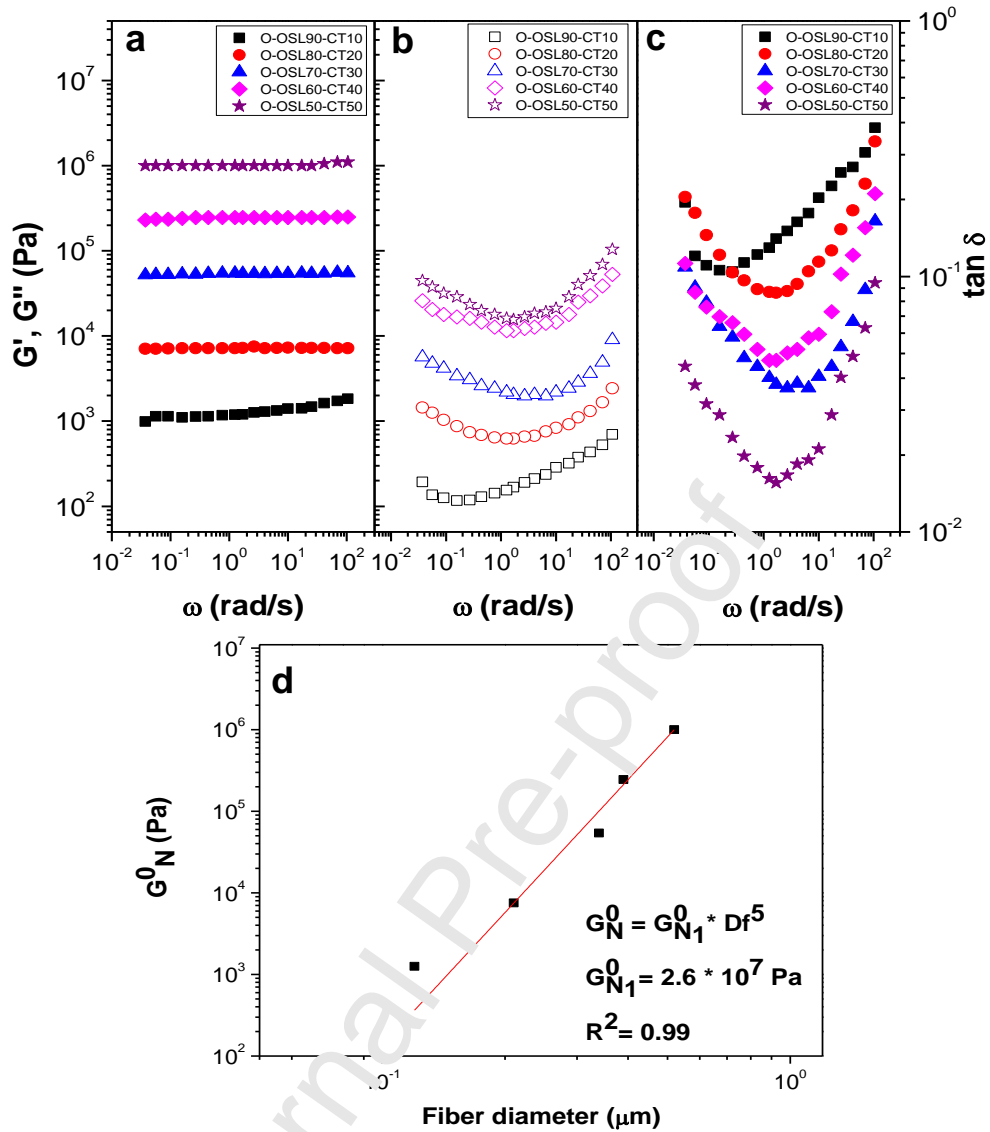


495  
 496 **Figure 6.** Frequency dependence of a) the storage ( $G'$ ) and loss ( $G''$ ) moduli and b) the  
 497 loss tangent, for gel-like dispersions prepared with the OSL90-CT10 nanostructure at 5, 10  
 498 and 15 wt.%.

499 Figure 7 illustrates the variation of the SAOS functions (viz., the storage modulus,  $G'$   
 500 and loss modulus,  $G''$ ) with frequency for gel-like dispersions prepared with variable

501 electrospun OSL:CT weight ratio (90:10 to 50:50). As can be seen, the SAOS functions  
502 frequency dependence is not qualitatively influenced by the electrospun OSL:CT nanostructure  
503 weight ratio in the frequency range studied. However,  $G'$  and  $G''$  increased markedly by  
504 decreasing OSL:CT weight ratio due to an increased proportion of the component with the  
505 higher average molecular weight (CT) in the nanostructure and morphological properties  
506 (higher average fiber). On the other hand, relative elasticity increases as the proportion of CT  
507 increases (Figure 7c). It should be noted that with an electrospun mats concentration of 5 wt.%  
508 and OSL:CT weight ratio of 90:10, 80:20 and 70:30 or 5, 10 and 15 wt % concentration and  
509 90:10 weight ratio is possible to obtain values of the viscoelastic functions comparable to those  
510 exhibited by conventional lubricating greases, with typical  $G'$  values of  $10^3$ - $10^5$  Pa depending  
511 on the thickener and concentration, and  $G''$  values around one order of magnitude lower  
512 [66,67]. Furthermore, these results are in agreement with those of other studies in which an  
513 increase in the dopant biopolymer proportion leads to an increase in SAOS functions [22,60].  
514 On the other hand, Borrego et al [27] and Rubio-Valle et al [38] obtained similar values of  
515 viscoelastic functions but at higher concentrations of thickener, developing electrospun low-  
516 sulfonate lignin/polyvinylpyrrolidone and eucalyptus Kraft lignin/cellulose acetate  
517 nanostructures, respectively, to structure castor oil.

518 In order to demonstrate the above-mentioned effect of electrospun nanostructure  
519 morphology on the viscoelastic response of gel-like dispersions, the plateau modulus ( $G_N^0$ ), as  
520 defined elsewhere [68], is plotted in Figure 7d as a function of mean fiber diameter, showing a  
521 power-law evolution with this parameter.



522

523 **Figure 7.** Frequency dependence of a) the storage modulus,  $G'$ , b) the loss modulus,  $G''$ , c)

524 the loss tangent, for gel-like dispersion prepared with variable OSL:CT weight ratio at 5 wt.%

525 and d) dependence of the plateau modulus with fiber diameter of nanostructure, for gel-like

526 dispersions prepared with variable OSL:CT weight ratio.

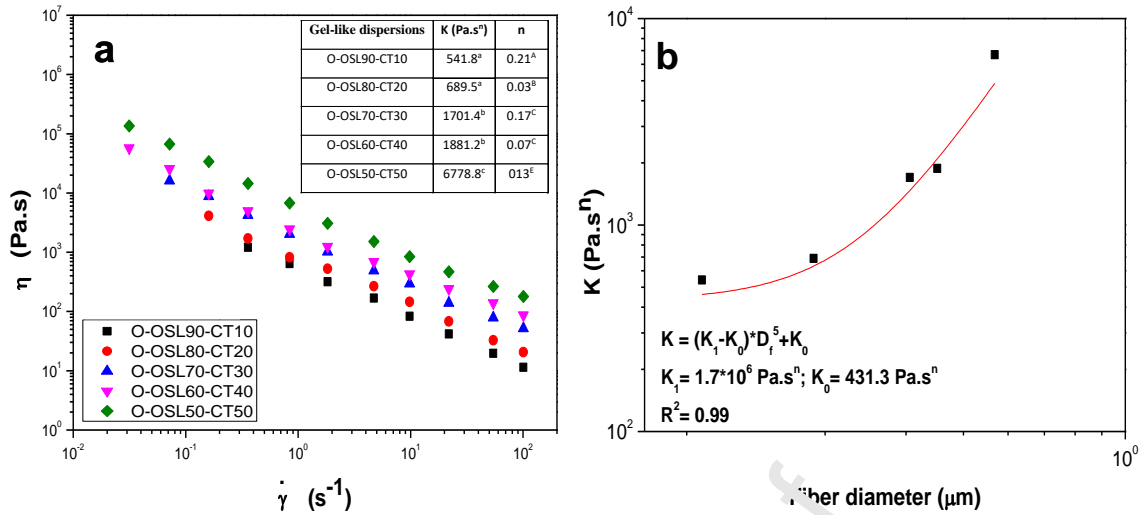
527 On the other hand, Figure 8a displays the viscous flow curves of OSL/CT nanofiber

528 structured gel-like dispersions as a function of the OSL:CT weight ratio. The power law model

529 adequately fits the shear thinning behavior:

530 
$$\eta = K \cdot \dot{\gamma}^{n-1} \quad (\text{eq 1})$$

531 where K and n are the consistency and the flow indexes, respectively.



532

533 **Figure 8.** a) Viscous flow curves and b) dependence of the consistency index (K) with  
 534 average fiber diameter for gel-like dispersions prepared with variable OSL:CT weight ratio.

535

536 The Table inside Figure 8a provides the values of both fitting parameters for the  
 537 different gel-like dispersions. Similarly to SAOS functions, K increased by decreasing OSL:CT  
 538 weight ratio and depends on the morphological properties of the electrospun OSL/CT  
 539 nanostructures. On the other hand, the low values of the flow index, n, reveal a shear-thinning  
 540 response, which is typical of materials with markedly non-Newtonian properties such as  
 541 conventional lubricating greases [67]. Figure 8b illustrates the relationship between K and the  
 542 mean fiber diameter and as can be seen, K potentially evolves with this parameter.

543

#### 544 4. Conclusions

545 Olive stones (OS) were submitted to a sequential acid/steam explosion  
 546 pretreatment, which was followed by a presaccharification, saccharification and simultaneous  
 547 saccharification and fermentation (PSSF) process of the pretreated material to obtain a liquid  
 548 media containing ethanol and a lignin-rich solid residue. This resulting OS lignin-rich residue  
 549 (OSL) displayed high lignin content along with some carbohydrate impurities. In addition, OSL

550 showed a predominance of  $\beta$ - $\beta'$  resinol substructures (42.1 % of the total inter-unit linkages),  
551 followed by  $\beta$ -O-4' alkyl aryl ethers (31.4 %), and  $\beta$ -5' phenylcoumaran substructures (17.3  
552 %), together with high molecular weight, and low S/G ratio and phenolic content. Subsequently,  
553 nanofibrous webs of OSL and cellulose triacetate (CT) were produced by electrospinning and  
554 the thickening ability of these in castor oil was verified. The morphology of electrospun  
555 OSL/CT nanostructures can be modulated by modifying the OSL:CT weight ratio and it is  
556 dependent on the intrinsic properties of the solution. Electrospun OSL/CT nanostructures were  
557 formed by filament-interconnected particles, BOAS, or well-developed uniform nanofiber. The  
558 linear viscoelastic response of the gel-like dispersions was qualitatively similar but SAOS  
559 functions increased with electrospun nanostructure concentration and CT proportion. The  
560 morphological characteristics of the electrospun nanostructures, i.e., the average fiber diameter  
561 significantly affect the viscous and viscoelastic properties of the resulting gel-like dispersions.

562

### 563 **Acknowledgments**

564 This work is a collaborative research of different projects: RTI2018- 096080-B-C21, RTI2018-  
565 096080-B-C22, PID2021-125657OB-I00, TED2021-132122B-C21 and ENE2017-85819-C2-  
566 2-R funded by MCIN/AEI/10.13039/501100011033 and by "ERDF A way of making Europe",  
567 SUSTEC-CM S2018/EMT-4348 project funded by Comunidad de Madrid. The authors  
568 gratefully acknowledge the aforementioned financial support. J.F.R.-V. additionally has  
569 received a Ph.D. Research Grant PRE2019-090632 from Spain's Ministry of Science and  
570 Innovation. The financial support is gratefully acknowledged.

571

572

573

574

575 **References**

- 576 [1] A. Susmozas, R. Martín-Sampedro, D. Ibarra, M.E. Eugenio, R. Iglesias, P. Manzanares,  
577 A.D. Moreno, Process Strategies for the Transition of 1G to Advanced Bioethanol  
578 Production, *Processes*. 8 (2020) 1310. <https://doi.org/10.3390/pr8101310>.
- 579 [2] A. Arevalo-Gallegos, Z. Ahmad, M. Asgher, R. Parra-Saldivar, H.M.N. Iqbal,  
580 Lignocellulose: A sustainable material to produce value-added products with a zero  
581 waste approach—A review, *Int. J. Biol. Macromol.* 99 (2017) 308–318.  
582 <https://doi.org/10.1016/j.ijbiomac.2017.02.097>.
- 583 [3] <https://www.fao.org/faostat/en/#data/QCL>.
- 584 [4] P. Doménech, A. Duque, I. Higuera, R. Iglesias, P. Manzanares, Biorefinery of the  
585 Olive Tree—Production of Sugars from Enzymatic Hydrolysis of Olive Stone Pretreated  
586 by Alkaline Extrusion, *Energies*. 13 (2020), 4517. <https://doi.org/10.3390/en13174517>.
- 587 [5] C. Padilla-Rascón, E. Ruiz, I. Romero, E. Castro, J.M. Oliva, I. Ballesteros, P.  
588 Manzanares, Valorisation of olive stone by-product for sugar production using a  
589 sequential acid/steam explosion pretreatment, *Ind. Crops Prod.* 148 (2020) 112279.  
590 <https://doi.org/10.1016/j.indcrop.2020.112279>.
- 591 [6] EU Dir. 2018/2001 Eur. Parliam. Counc. 11 December 2018 Promot. Use Energy from  
592 Renew. Sources, Eur. Parliam. Counc. Eur. Union Brussels, Belgium, 2018, n.d.  
593 <https://doi.org/https://eur-lex.europa.eu/eli/dir/2018/2001/oj>.
- 594 [7] T. Raj, K. Chandrasekhar, A. Naresh Kumar, J. Rajesh Banu, J.-J. Yoon, S. Kant Bhatia,  
595 Y.-H. Yang, S. Varjani, S.-H. Kim, Recent advances in commercial biorefineries for  
596 lignocellulosic ethanol production: Current status, challenges and future perspectives,  
597 *Bioresour. Technol.* 344 (2022) 126292. <https://doi.org/10.1016/j.biortech.2021.126292>.
- 598 [8] A.J. Ragauskas, G.T. Beckham, M.J. Biddy, R. Chandra, F. Chen, M.F. Davis, B.H.  
599 Davison, R.A. Dixon, P. Gilna, M. Keller, P. Langan, A.K. Naskar, J.N. Saddler, T.J.

- 600 Tschaplinski, G.A. Tuskan, C.E. Wyman, Lignin Valorization: Improving Lignin  
601 Processing in the Biorefinery, *Science* (80-. ). 344 (2014).  
602 <https://doi.org/10.1126/science.1246843>.
- 603 [9] J. Ralph, K. Lundquist, G. Brunow, F. Lu, H. Kim, P.F. Schatz, J.M. Marita, R.D.  
604 Hatfield, S.A. Ralph, J.H. Christensen, W. Boerjan, Lignins: Natural polymers from  
605 oxidative coupling of 4-hydroxyphenyl- propanoids, *Phytochem. Rev.* 3 (2004) 29–60.  
606 <https://doi.org/10.1023/B:PHYT.0000047809.65444.a4>.
- 607 [10] P. Azadi, O.R. Inderwildi, R. Farnood, D.A. King, Liquid fuels, hydrogen and chemicals  
608 from lignin: A critical review, *Renew. Sustain. Energy Rev.* 21 (2013) 506–523.  
609 <https://doi.org/10.1016/j.rser.2012.12.022>.
- 610 [11] A.M. Borrero-López, F.J. Santiago-Medina, C. Valencia, M.E. Eugenio, R. Martín-  
611 Sampedro, J.M. Franco, Valorization of Lignin as Thickener in Castor Oil for  
612 Lubricant Applications, *J. Renew. Mater.* 6 (2018) 347–361.  
613 <https://doi.org/10.7569/JRM.2017.634160>.
- 614 [12] T. Shahzadi, S. Mehmood, M. Farhad, Z. Anwar, A. Afroz, N. Zeeshan, U. Rashid, K.  
615 Sughra, Advances in lignocellulosic biotechnology: A brief review on lignocellulosic  
616 biomass and celluloses, *Adv. Biosci. Biotechnol.* 05 (2014) 246–251.  
617 <https://doi.org/10.4236/abb.2014.53031>.
- 618 [13] N. Núñez, J.E. Martín-Alfonso, C. Valencia, M.C. Sánchez, J.M. Franco, Rheology of  
619 new green lubricating grease formulations containing cellulose pulp and its methylated  
620 derivative as thickener agents, *Ind. Crops Prod.* 37 (2012) 500–507.  
621 <https://doi.org/10.1016/j.indcrop.2011.07.027>.
- 622 [14] R. Gallego, J.F. Arteaga, C. Valencia, J.M. Franco, Rheology and thermal degradation  
623 of isocyanate-functionalized methyl cellulose-based oleogels, *Carbohydr. Polym.* 98  
624 (2013) 152–160. <https://doi.org/10.1016/j.carbpol.2013.04.104>.

- 625 [15] M. Trejo-Cáceres, M.C. Sánchez, J.E. Martín-Alfonso, Impact of acetylation process of  
626 kraft lignin in development of environment-friendly semisolid lubricants, *Int. J. Biol.*  
627 *Macromol.* 227 (2023) 673–684. <https://doi.org/10.1016/j.ijbiomac.2022.12.096>.
- 628 [16] T.M. Panchal, A. Patel, D.D. Chauhan, M. Thomas, J. V. Patel, A methodological review  
629 on bio-lubricants from vegetable oil based resources, *Renew. Sustain. Energy Rev.* 70  
630 (2017) 65–70. <https://doi.org/10.1016/j.rser.2016.11.105>.
- 631 [17] A.Z. Syahir, N.W.M. Zulkifli, H.H. Masjuki, M.A. Kalam, A. Alabdulkarem, M. Gulzar,  
632 L.S. Khuong, M.H. Harith, A review on bio-based lubricants and their applications, *J.*  
633 *Clean. Prod.* 168 (2017) 997–1016. <https://doi.org/10.1016/j.jclepro.2017.09.106>.
- 634 [18] A.M. Borrero-López, R. Martín-Sampedro, D. Jharia, C. Valencia, M.E. Eugenio, J.M.  
635 Franco, Evaluation of lignin-enriched side-streams from different biomass conversion  
636 processes as thickeners in bio-lubricant formulations, *Int. J. Biol. Macromol.* 162 (2020)  
637 1398–1413. <https://doi.org/10.1016/j.ijbiomac.2020.07.292>.
- 638 [19] A.M. Borrero-López, C. Valencia, J.M. Franco, Lignocellulosic Materials for the  
639 Production of Biofuels, Biochemicals and Biomaterials and Applications of  
640 Lignocellulose-Based Polyurethanes: A Review, *Polymers (Basel)*. 14 (2022) 881.  
641 <https://doi.org/10.3390/polym14050881>.
- 642 [20] E. Cortés-Triviño, C. Valencia, M.A. Delgado, J.M. Franco, Rheology of epoxidized  
643 cellulose pulp gel-like dispersions in castor oil: Influence of epoxidation degree and the  
644 epoxide chemical structure, *Carbohydr. Polym.* 199 (2018) 563–571.  
645 <https://doi.org/10.1016/j.carbpol.2018.07.058>.
- 646 [21] E. Cortés-Triviño, C. Valencia, J.M. Franco, Influence of epoxidation conditions on the  
647 rheological properties of gel-like dispersions of epoxidized kraft lignin in castor oil,  
648 *Holzforschung*. 71 (2017) 777–784. <https://doi.org/10.1515/hf-2017-0012>.
- 649 [22] J.F. Rubio-Valle, M.C. Sánchez, C. Valencia, J.E. Martín-Alfonso, J.M. Franco,

- 650 Electrohydrodynamic Processing of PVP-Doped Kraft Lignin Micro- and Nano-  
651 Structures and Application of Electrospun Nanofiber Templates to Produce Oleogels,  
652 *Polymers (Basel)*. 13 (2021) 2206. <https://doi.org/10.3390/polym13132206>.
- 653 [23] J.F. Rubio-Valle, C. Valencia, M. Sánchez, J.E. Martín-Alfonso, J.M. Franco, Oil  
654 structuring properties of electrospun Kraft lignin/cellulose acetate nanofibers for  
655 lubricating applications: influence of lignin source and lignin/cellulose acetate ratio,  
656 *Cellulose*. 30 (2023) 1553–1566. <https://doi.org/10.1007/s10570-022-04963-2>.
- 657 [24] M. Borrego, J.E. Martín-Alfonso, C. Valencia, M.C. Sánchez, J.M. Franco, Impact of  
658 the Morphology of Electrospun Lignin/Ethylcellulose Nanostructures on Their Capacity  
659 to Thicken Castor Oil, *Polymers (Basel)*. 14 (2022) 4741.  
660 <https://doi.org/10.3390/polym14214741>.
- 661 [25] J.F. Rubio-Valle, M. Jiménez-Rosado, V. Jerez-Puyana, A. Guerrero, A. Romero,  
662 Electrospun nanofibres with antimicrobial activities, in: *Antimicrob. Text. from Nat.*  
663 *Resour.*, Elsevier, 2021: pp. 589–618. [https://doi.org/10.1016/B978-0-12-821485-](https://doi.org/10.1016/B978-0-12-821485-5.00020-2)  
664 [5.00020-2](https://doi.org/10.1016/B978-0-12-821485-5.00020-2).
- 665 [26] I. Dallmeyer, F. Ko, J.F. Kadla, Correlation of Elongational Fluid Properties to Fiber  
666 Diameter in Electrospinning of Softwood Kraft Lignin Solutions, *Ind. Eng. Chem. Res.*  
667 53 (2014) 2697–2705. <https://doi.org/10.1021/ie403724y>.
- 668 [27] M. Borrego, J.E. Martín-Alfonso, M.C. Sánchez, C. Valencia, J.M. Franco, Electrospun  
669 lignin-PVP nanofibers and their ability for structuring oil, *Int. J. Biol. Macromol.* 180  
670 (2021) 212–221. <https://doi.org/10.1016/j.ijbiomac.2021.03.069>.
- 671 [28] I. Dallmeyer, F. Ko, J.F. Kadla, Electrospinning of Technical Lignins for the Production  
672 of Fibrous Networks, *J. Wood Chem. Technol.* 30 (2010) 315–329.  
673 <https://doi.org/10.1080/02773813.2010.527782>.
- 674 [29] I. Dallmeyer, L.T. Lin, Y. Li, F. Ko, J.F. Kadla, Preparation and Characterization of

- 675 Interconnected, Kraft Lignin-Based Carbon Fibrous Materials by Electrospinning,  
676 *Macromol. Mater. Eng.* 299 (2014) 540–551. <https://doi.org/10.1002/mame.201300148>.
- 677 [30] L. García-Fuentevilla, J.F. Rubio-Valle, R. Martín-Sampedro, C. Valencia, M.E.  
678 Eugenio, D. Ibarra, Different Kraft lignin sources for electrospun nanostructures  
679 production: Influence of chemical structure and composition, *Int. J. Biol. Macromol.* 214  
680 (2022) 554–567. <https://doi.org/10.1016/j.ijbiomac.2022.06.121>.
- 681 [31] D. Ibarra, L. García-Fuentevilla, J.F. Rubio-Valle, R. Martín-Sampedro, C. Valencia,  
682 M.E. Eugenio, Kraft lignins from different poplar genotypes obtained by selective acid  
683 precipitation and their use for the production of electrospun nanostructures, *React. Funct.*  
684 *Polym.* 191 (2023) 105685. <https://doi.org/10.1016/j.reactfunctpolym.2023.105685>.
- 685 [32] M.A. Teixeira, M.C. Paiva, M.T.P. Amorim, H.P. Felgueiras, Electrospun  
686 nanocomposites containing cellulose and its derivatives modified with specialized  
687 biomolecules for an enhanced wound healing, *Nanomaterials.* 10 (2020).  
688 <https://doi.org/10.3390/nano10030557>.
- 689 [33] P. Sánchez-Cid, J.F. Rubio-Valle, M. Jiménez-Rosado, V. Pérez-Puyana, A. Romero,  
690 Effect of Solution Properties in the Development of Cellulose Derivative Nanostructures  
691 Processed via Electrospinning, *Polymers (Basel).* 14 (2022) 665.  
692 <https://doi.org/10.3390/polym14040665>.
- 693 [34] R. Konwarh, N. Karak, M. Misra, Electrospun cellulose acetate nanofibers: The present  
694 status and gamut of biotechnological applications, *Biotechnol. Adv.* 31 (2013) 421–437.  
695 <https://doi.org/10.1016/j.biotechadv.2013.01.002>.
- 696 [35] L.A. Quinchia, M.A. Delgado, C. Valencia, J.M. Franco, C. Gallegos, Viscosity  
697 modification of different vegetable oils with EVA copolymer for lubricant applications,  
698 *Ind. Crops Prod.* 32 (2010) 607–612. <https://doi.org/10.1016/j.indcrop.2010.07.011>.
- 699 [36] J.B. Sluiter, R.O. Ruiz, C.J. Scarlata, A.D. Sluiter, D.W. Templeton, Compositional

- 700 Analysis of Lignocellulosic Feedstocks. 1. Review and Description of Methods, *J. Agric.*  
701 *Food Chem.* 58 (2010) 9043–9053. <https://doi.org/10.1021/jf1008023>.
- 702 [37] L. Jiménez-López, R. Martín-Sampedro, M.E. Eugenio, J.I. Santos, H. Sixto, I. Cañellas,  
703 D. Ibarra, Co-production of soluble sugars and lignin from short rotation white poplar  
704 and black locust crops, *Wood Sci. Technol.* 54 (2020) 1617–1643.  
705 <https://doi.org/10.1007/s00226-020-01217-x>.
- 706 [38] J.F. Rubio-Valle, M.C. Sánchez, C. Valencia, J.E. Martín-Alfonso, J.M. Franco,  
707 Production of lignin/cellulose acetate fiber-bead structures by electrospinning and  
708 exploration of their potential as green structuring agents for vegetable lubricating oils,  
709 *Ind. Crops Prod.* 188 (2022) 115579. <https://doi.org/10.1016/j.indcrop.2022.115579>.
- 710 [39] A.D. Moreno, L. Olsson, Pretreatment of Lignocellulosic Feedstocks, in: *Extrem.*  
711 *Enzym. Process. Lignocellul. Feed. to Bioenergy*, Springer International Publishing,  
712 Cham, 2017: pp. 31–52. [https://doi.org/10.1007/978-3-319-54684-1\\_3](https://doi.org/10.1007/978-3-319-54684-1_3).
- 713 [40] P. Alvira, M. Ballesteros, M.J. Negro, Progress on Enzymatic Saccharification  
714 Technologies for Biofuels Production, in: *Biofuel Technol.*, Springer Berlin Heidelberg,  
715 Berlin, Heidelberg, 2013 pp. 145–169. [https://doi.org/10.1007/978-3-642-34519-7\\_6](https://doi.org/10.1007/978-3-642-34519-7_6).
- 716 [41] M.Á.B. Alcántara, J. Dobruchowska, P. Azadi, B.D. García, F.P. Molina-Heredia, F.M.  
717 Reyes-Sosa, Recalcitrant carbohydrates after enzymatic hydrolysis of pretreated  
718 lignocellulosic biomass, *Biotechnol. Biofuels.* 9 (2016) 207.  
719 <https://doi.org/10.1186/s13068-016-0629-4>.
- 720 [42] J.I. Santos, R. Martín-Sampedro, Ú. Fillat, J.M. Oliva, M.J. Negro, M. Ballesteros, M.E.  
721 Eugenio, D. Ibarra, Evaluating Lignin-Rich Residues from Biochemical Ethanol  
722 Production of Wheat Straw and Olive Tree Pruning by FTIR and 2D-NMR, *Int. J. Polym.*  
723 *Sci.* 2015 (2015) 1–11. <https://doi.org/10.1155/2015/314891>.
- 724 [43] J.I. Santos, Ú. Fillat, R. Martín-Sampedro, M.E. Eugenio, M.J. Negro, I. Ballesteros, A.

- 725 Rodríguez, D. Ibarra, Evaluation of lignins from side-streams generated in an olive tree  
726 pruning-based biorefinery: Bioethanol production and alkaline pulping, *Int. J. Biol.*  
727 *Macromol.* 105 (2017) 238–251. <https://doi.org/10.1016/j.ijbiomac.2017.07.030>.
- 728 [44] A.M. Borrero-López, C. Valencia, D. Ibarra, I. Ballesteros, J.M. Franco, Lignin-enriched  
729 residues from bioethanol production: Chemical characterization, isocyanate  
730 functionalization and oil structuring properties, *Int. J. Biol. Macromol.* 195 (2022) 412–  
731 423. <https://doi.org/10.1016/j.ijbiomac.2021.11.185>.
- 732 [45] M. Alekhina, O. Ershova, A. Ebert, S. Heikkinen, H. Sixta, Softwood kraft lignin for  
733 value-added applications: Fractionation and structural characterization, *Ind. Crops Prod.*  
734 66 (2015) 220–228. <https://doi.org/10.1016/j.indcrop.2014.12.021>.
- 735 [46] D. Ibarra, J.C. de Río, A. Gutiérrez, I.M. Rodríguez, J. Romero, M.J. Martínez, Á.T.  
736 Martínez, Isolation of high-purity residual lignans from eucalypt paper pulps by cellulase  
737 and proteinase treatments followed by solvent extraction, *Enzyme Microb. Technol.* 35  
738 (2004) 173–181. <https://doi.org/10.1016/j.enzmictec.2004.04.002>.
- 739 [47] J. Li, G. Henriksson, G. Gellerstedt, Lignin depolymerization/repolymerization and its  
740 critical role for delignification of aspen wood by steam explosion, *Bioresour. Technol.*  
741 98 (2007) 3061–3068. <https://doi.org/10.1016/j.biortech.2006.10.018>.
- 742 [48] R. Samuel, M. Foston, N. Jaing, S. Cao, L. Allison, M. Studer, C. Wyman, A.J.  
743 Ragauskas, HSQC (heteronuclear single quantum coherence)  $^{13}\text{C}$ – $^1\text{H}$  correlation  
744 spectra of whole biomass in perdeuterated pyridinium chloride–DMSO system: An  
745 effective tool for evaluating pretreatment, *Fuel.* 90 (2011) 2836–2842.  
746 <https://doi.org/10.1016/j.fuel.2011.04.021>.
- 747 [49] S. Heikkinen, M.M. Toikka, P.T. Karhunen, I.A. Kilpeläinen, Quantitative 2D HSQC  
748 (Q-HSQC) via Suppression of J -Dependence of Polarization Transfer in NMR  
749 Spectroscopy: Application to Wood Lignin, *J. Am. Chem. Soc.* 125 (2003) 4362–4367.

- 750 <https://doi.org/10.1021/ja029035k>.
- 751 [50] H. Wang, Z. Liu, L. Hui, L. Ma, X. Zheng, J. Li, Y. Zhang, Understanding the structural  
752 changes of lignin in poplar following steam explosion pretreatment, *Holzforschung*. 74  
753 (2020) 275–285. <https://doi.org/10.1515/hf-2019-0087>.
- 754 [51] J. Rencoret, A. Gutiérrez, E. Castro, J.C. del Río, Structural characteristics of lignin in  
755 pruning residues of olive tree ( *Olea europaea* L.), *Holzforschung*. 73 (2018) 25–34.  
756 <https://doi.org/10.1515/hf-2018-0077>.
- 757 [52] F. Araya, E. Troncoso, R.T. Mendonça, J. Freer, Condensed lignin structures and re-  
758 localization achieved at high severities in autohydrolysis of *Eucalyptus globulus* wood  
759 and their relationship with cellulose accessibility. *Bio-technol. Bioeng.* 112 (2015) 1783–  
760 1791. <https://doi.org/10.1002/bit.25604>.
- 761 [53] A. Lourenço, S. Araújo, J. Gominho, H. Pereira, D. Evtuguin, Structural changes in  
762 lignin of thermally treated eucalyptus wood, *J. Wood Chem. Technol.* 40 (2020) 258–  
763 268. <https://doi.org/10.1080/02773813.2020.1769674>.
- 764 [54] S.O. Prozil, D. V. Evtuguin, A.M.S. Silva, L.P.C. Lopes, Structural Characterization of  
765 Lignin from Grape Stalks ( *Vitis vinifera* L.), *J. Agric. Food Chem.* 62 (2014) 5420–  
766 5428. <https://doi.org/10.1021/jf502267s>.
- 767 [55] C. Padilla-Rascón, E. Ruiz, E. Castro, L.B. Roseiro, L.C. Duarte, F. Carvalheiro,  
768 Effective Production of Bioactive Phenolic Compounds from Olive Stones, in: 2nd Int.  
769 Electron. Conf. Foods - “Future Foods Food Technol. a Sustain. World,” MDPI, Basel  
770 Switzerland, 2021: p. 70. <https://doi.org/10.3390/Foods2021-10940>.
- 771 [56] J. Rencoret, G. Marques, A. Gutiérrez, D. Ibarra, J. Li, G. Gellerstedt, J.I. Santos, J.  
772 Jiménez-Barbero, Á.T. Martínez, J.C. del Río, Structural characterization of milled wood  
773 lignins from different eucalypt species, *Holzforschung*. 62 (2008).  
774 <https://doi.org/10.1515/HF.2008.096>.

- 775 [57] M.E. Eugenio, R. Martín-Sampedro, J.I. Santos, B. Wicklein, D. Ibarra, Chemical,  
776 Thermal and Antioxidant Properties of Lignins Solubilized during Soda/AQ Pulping of  
777 Orange and Olive Tree Pruning Residues, *Molecules*. 26 (2021) 3819.  
778 <https://doi.org/10.3390/molecules26133819>.
- 779 [58] R. Martín-Sampedro, J.I. Santos, M.E. Eugenio, B. Wicklein, L. Jiménez-López, D.  
780 Ibarra, Chemical and thermal analysis of lignin streams from *Robinia pseudoacacia* L.  
781 generated during organosolv and acid hydrolysis pre-treatments and subsequent  
782 enzymatic hydrolysis, *Int. J. Biol. Macromol.* 140 (2019) 311–322.  
783 <https://doi.org/10.1016/j.ijbiomac.2019.08.029>.
- 784 [59] A. Tolbert, H. Akinosho, R. Khunsupat, A.K. Naskar, A.J. Ragauskas, Characterization  
785 and analysis of the molecular weight of lignin for biorefining studies, *Biofuels, Bioprod.*  
786 *Biorefining*. 8 (2014) 836–856. <https://doi.org/10.1002/bbb.1500>.
- 787 [60] M. Borrego, J.E. Martín-Alfonso, J. Valencia, M. del C. Sánchez Carrillo, J.M. Franco,  
788 Developing Electrospun Ethylcellulose Nanofibrous Webs: An Alternative Approach for  
789 Structuring Castor Oil, *ACS Appl. Polym. Mater.* 4 (2022) 7217–7227.  
790 <https://doi.org/10.1021/acssapm.2c01090>.
- 791 [61] N. Alwadani, N. Ghannem, P. Fatehi, Surface and interface characteristics of  
792 hydrophobic lignin derivatives in solvents and films, *Colloids Surfaces A Physicochem.*  
793 *Eng. Asp.* 609 (2021) 125656. <https://doi.org/10.1016/j.colsurfa.2020.125656>.
- 794 [62] S. Kubo, J.F. Kadla, Hydrogen Bonding in Lignin: A Fourier Transform Infrared Model  
795 Compound Study, *Biomacromolecules*. 6 (2005) 2815–2821.  
796 <https://doi.org/10.1021/bm050288q>.
- 797 [63] M.A. Martín-Alfonso, J.F. Rubio-Valle, J.P. Hinestroza, J.E. Martín-Alfonso, Impact of  
798 Vegetable Oil Type on the Rheological and Tribological Behavior of Montmorillonite-  
799 Based Oleogels, *Gels*. 8 (2022) 504. <https://doi.org/10.3390/gels8080504>.

- 800 [64] R. Gallego, J.F. Arteaga, C. Valencia, M.J. Díaz, J.M. Franco, Gel-Like Dispersions of  
801 HMDI-Cross-Linked Lignocellulosic Materials in Castor Oil: Toward Completely  
802 Renewable Lubricating Grease Formulations, *ACS Sustain. Chem. Eng.* 3 (2015) 2130–  
803 2141. <https://doi.org/10.1021/acssuschemeng.5b00389>.
- 804 [65] E. Cortés-Triviño, C. Valencia, M.A. Delgado, J.M. Franco, Thermo-rheological and  
805 tribological properties of novel bio-lubricating greases thickened with epoxidized  
806 lignocellulosic materials, *J. Ind. Eng. Chem.* 80 (2019) 626–632.  
807 <https://doi.org/10.1016/j.jiec.2019.08.052>.
- 808 [66] R. Sánchez, C. Valencia, J.M. Franco, Rheological and Tribological Characterization of  
809 a New Acylated Chitosan-Based Biodegradable Lubricating Grease: A Comparative  
810 Study with Traditional Lithium and Calcium Greases, *Tribol. Trans.* 57 (2014) 445–454.  
811 <https://doi.org/10.1080/10402004.2014.383541>.
- 812 [67] M.A. Delgado, C. Valencia, M.C. Sánchez, J.M. Franco, C. Gallegos,  
813 Thermorheological behaviour of a lithium lubricating grease, *Tribol. Lett.* 23 (2006) 47–  
814 54. <https://doi.org/10.1007/s11249-006-9109-5>.
- 815 [68] J.D. Ferry, *Viscoelastic properties of polymers*, 3rd ed., New York, 1980.  
816  
817

## Highlights

818  
819

820 Valorization of lignin-rich residue from the bioethanol production of olive stones

821 Lignin-rich residue presented the main inter-unit linkages and low S/G ratios

822 Electrospinning of lignin-rich residue (OSL) and cellulose triacetate (CT)

823 Castor oil structuring ability of electrospun OSL/CT nanostructures

824 Rheological properties of gel-like dispersions tuned by OSL/CA weight ratio

Journal Pre-proof